Inference and Planning with Virtual and Physical Constraints for Object Manipulation

João Loula
Department of Brain and Computer Sciences
Massachusetts Institute of Technology United States
jloula@mit.edu

Kelsey R. Allen
Department of Brain and Computer Sciences
Massachusetts Institute of Technology United States
krallen@mit.edu

Alberto Rodriguez
Department of Mechanical Engineering
MIT United States
albertor@mit.edu

Joshua B. Tenenbaum
Department of Brain and Computer Sciences
MIT United States
jbt@mit.edu

Nima Fazeli
Department of Mechanical Engineering
University of Michigan United States
nfz@umich.edu

Abstract: Object manipulation is a challenging long-horizon planning task. To address this challenge, tasks are typically decomposed into a sequence of phases and primitives. We propose a framework for manipulation that decomposes tasks into kinematic graphs comprised of virtual and physical kinematic constraints. To this end, we first infer a set of producible constraints during an exploration phase. Next, we demonstrate an efficient planning procedure that uses kinematic graphs built from these constraints for object manipulation. We conclude by showing generalization across tool-object interactions by virtue of object-centric encoding of the constraints.

Keywords: Planning, Manipulation, Representation Learning

1 Introduction

Making and breaking contact is characteristic of sequential manipulation tasks: the resulting discontinuous mechanics pose a challenge for planning. This challenge can be effectively addressed by decomposing the problem into a sequence of phases, each represented by a hand-engineered abstraction [1–7]. How these abstractions generalize to novel scenarios, however, is unclear, as the original problem decomposition could no longer be relevant. How can we represent planning abstractions such that they're general enough to tackle new problems, but constrained enough to allow efficient learning?

Consider the task of pushing a block to the goal configuration depicted in Figure 1 (third pane). One way to solve this task is to use a model of the dynamics of pushing, either analytical (e.g. [8]) or learned (e.g. [9]): in either case the models are complex, and planning with them is difficult. Alternatively, one might reason that within the set of all pushes, a few of them reliably create simple motions: the block moves in a straight line if it is pushed straight and close to the center, and it rotates if it is pushed close to the edge. Research in cognitive science tells us people systematically avoid reasoning about Newtonian mechanics in favor of such simple kinematic primitives [10–12]: these simplifications might be key for fast learning and generalizable planning.

We present a modelling and planning framework that learns kinematic graphs comprised of virtual and physical constraints, and uses them to decompose planning problems. We show that the model can generate the data it needs through simple grid-search policies for interacting with objects (Section 2.1), that it can repurpose efficient algorithms originally used for inferring joints in multi-link

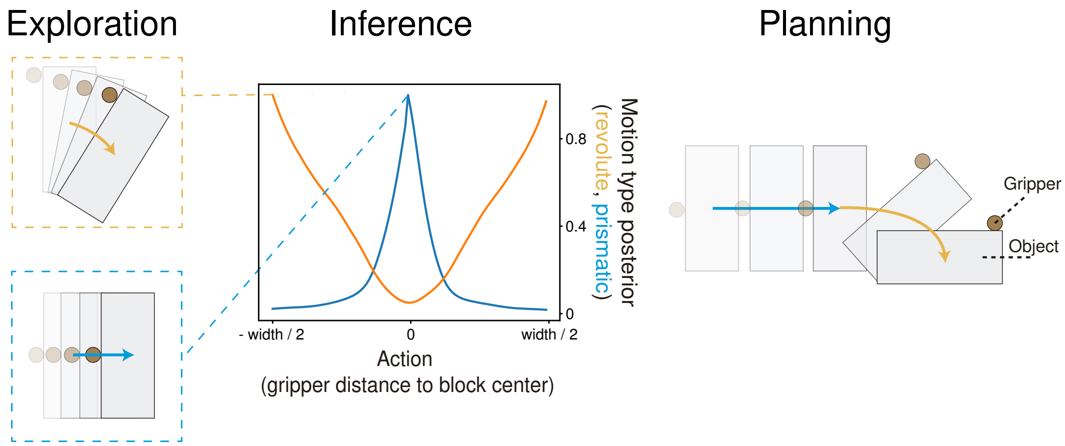

Figure 1: **Exploration:** the robot interacts with the block by pushing it along varying locations and directions, in a grid search fashion. **Inference:** the robot infers that some pushes move the block as though it were constrained by a virtual prismatic or revolute joint. **Planning:** The goal of the robot is to push the block to a desired configuration. The robot plans to achieve its goal by sequencing the learned constrained motions: first sliding, then rotating.

objects [13–15] to solve its learning problem (Section 2.2), and that the learned representations can be directly plugged into standard constraint-based task and motion planning [6] (Section 2.3).

We demonstrate the efficacy and flexibility of this approach for several challenging object manipulation tasks involving tool use (Section 3, see Figure 3 for the tasks considered). Crucially, though our model gets experience with the dynamics of tools during its exploration phase, it never sees tools being used on other objects—instead leveraging object-centric representations to discover these behaviors at test time. We conclude by reviewing related work and discussing limitations and future directions.

2 Framework

Our approach to object manipulation has three components: exploration, inference, and planning. During exploration, the robot attempts interactions with objects in the scene one at a time—such as poking a block or grasping a stick. During inference, it uses data from these interactions to discover realizable *affordances*, composed of virtual and physical constraints. Finally, during planning, the robot uses these constraints to search for sequences of actions to achieve desired goals. We detail these components in the following subsections.

2.1 Exploration

In the exploration phase the robot interacts with one object at a time, performing actions in order to discover which of these actions generate behavior that is well-described by simple kinematic abstractions. Actions consist of a position on the object where the robot will make contact as well a force to be applied at that contact:

$$\boldsymbol{a} = (\boldsymbol{p}, \boldsymbol{f}) \tag{1}$$

The robot searches over actions using an exploration policy—in this paper, we use a fixed grid search, but the policy could also be based on random search or active learning (e.g. [16]), for instance.

We are interested in tracking the trajectories that result, in particular the transform $\mathbf{T_{ro}}$ relating a fixed frame on the robot to a fixed frame on the target object, and the transform $\mathbf{T_{ow}}$ relating a fixed frame on the object to a fixed world frame; we call that trajectory $\mathbf{D}$:

$$\mathbf{D} = \left\{\mathbf{D^t}\right\} = \left\{\mathbf{T^t_{ro}}, \mathbf{T^t_{ow}}\right\} \tag{2}$$

2.2 Constraint Inference

In the inference phase, the robot takes the trajectories $\{\mathbf{D^t}\}$ from the exploration trials and attempts to model both the geometric relationship between robot and object $\mathbf{T^t_{ro}}$ and that between object and environment $\mathbf{T^t_{ow}}$ as stemming from simple kinematic constraints: these constraints will represent actions the robot can take and motions that result, respectively. Well call this representation that combines action and motion an *affordance*: the main insight for inference is that affordances can be inferred as the most likely kinematic graph having the robot r, the object o, and the environment w as nodes (see [13]). We note that this is a significant departure from the original use case of kinematic graph inference, which is to infer physical joints in multi-link objects, like a drawer moving on its slides, or a door rotating around its hinge. Here, we're using these algorithms to infer *virtual* joints: motion that is well-described by these constraints, even though there are no external mechanisms enforcing them.

Let $\boldsymbol{A}$ denote a possible kinematic graph with r, o, and w as vertices. To infer which affordance best describes a trajectory $\mathbf{D}$, we compute the posterior distribution over such graphs $\boldsymbol{A}$ conditioned on $\mathbf{D}$ by applying Bayes rule:

$$p(\boldsymbol{A}|\mathbf{D}) \propto p(\mathbf{D}|\boldsymbol{A})p(\boldsymbol{A}) \tag{3}$$

Note that the kinematic relationship between the three bodies is fully specified by giving two vertices (since the third constraint can be derived by composing the other two.)—as such, we represent the kinematic graph in the exploration trial by one edge $E_{r,o}$ between the robot and object nodes and one edge $E_{o,w}$ between object and environment: these correspond respectively to the affordance action and motion. We represent the constraint type of these two edges as $\boldsymbol{C}_{g,o}$ and $\boldsymbol{C}_{o,w}$, and they can be prismatic, revolute, fixed, or free. Each of these constraint types has its own set of parameters, such as the axis for a prismatic constraint, or the relative position for a fixed constraint. We'll represent the parameters for the action and motion constraints as $\boldsymbol{\theta}_{r,o}$ and $\boldsymbol{\theta}_{o,w}$, respectively (following Barragän et al. [14]). We can then compute the most likely graph for a given exploration trial as:

$$\begin{aligned}\hat{\boldsymbol{A}} &= \underset{\boldsymbol{A}}{\operatorname{argmax}}\ p(\mathbf{D}|\boldsymbol{A}) \\ &= \underset{\boldsymbol{A}}{\operatorname{argmax}}\ p(\mathbf{T_{r,o}}|\boldsymbol{C}_{r,o}, \boldsymbol{\theta}_{r,o})p(\mathbf{T_{o,w}}|\boldsymbol{C}_{o,w}, \boldsymbol{\theta}_{o,w})\end{aligned} \tag{4}$$

The last equality holds because a kinematic tree's edges are independent of each other. Sturm et al. [13] note that this allows for an efficient procedure for inferring the kinematic graph: first we compute the most likely type of constraint and parameters $(\boldsymbol{C}_{i,j}, \boldsymbol{\theta}_{i,j})$ for both pairs of bodies, and those will then constitute the most likely set of edges $\boldsymbol{E}$ composing the tree. The best constraint type and set of parameters to describe the interaction between two bodies i and j is given by (we omit the body indices for notation clarity):

$$(\hat{\boldsymbol{C}}, \hat{\boldsymbol{\theta}}) = \underset{\boldsymbol{C},\boldsymbol{\theta}}{\operatorname{argmax}}\ p(\boldsymbol{C}, \boldsymbol{\theta}|\mathbf{T}) \tag{5}$$

To solve equation 5, we consider each constraint type and compute its most likely parameters:

$$\hat{\boldsymbol{\theta}}_{\boldsymbol{C}} = \underset{\boldsymbol{\theta}}{\operatorname{argmax}}\ p(\boldsymbol{\theta}|\mathbf{T}, \boldsymbol{C})\ \propto\ p(\mathbf{T}|\boldsymbol{C}, \boldsymbol{\theta})p(\boldsymbol{\theta}|\boldsymbol{C}) \tag{6}$$

where $p(\boldsymbol{\theta}|\boldsymbol{C})$ is a prior over a joint's parameters, and $p(\mathbf{T}|\boldsymbol{\theta}, \boldsymbol{C})$ is the likelihood of a sequence of relative transforms given a parameterized constraint (we discuss the constraint models $\boldsymbol{C}$ in more detail in the appendix). Next, we use the computed most likely parameters from equation 6 to estimate the maximum a posteriori (MAP) of the constraint type:

$$\hat{\boldsymbol{C}} = \underset{\boldsymbol{C}}{\operatorname{argmax}}\ p(\hat{\boldsymbol{C}}|\mathbf{T}, \hat{\boldsymbol{\theta}}_{\boldsymbol{C}}) \tag{7}$$

The MAP constraint types inferred from equation 7 are then plugged into equation 4 to compute the graph likelihood. For planning, we keep only the affordances associated with the highest-likelihood graphs across exploration trials for each object.

A crucial advantage of the affordance representation is that it can easily be made agnostic to the effector used. Consider again the example of pushing a block along its center of mass: the affordance here consists of a constraint $C_{o,w}$ describing the robot's sliding motion and a constraint $C_{r,o}$

describing the action as a required geometric relationship between a fixed frame on the robot and a fixed frame on the object, (for instance, between the tip of the robot's finger and the block's center of mass). But $C_{r,o}$ could also describe the relationship between e.g. a stick and the block, provided one can define a frame on the stick that has similar geometric properties to the tip of the robot's finger. In this work, we suppose that such a correspondence is known, and show that that allows us to enact learned affordances with tools without previous experience using tools on objects (more details in Section 3). In Section 5 we discuss this assumption and the possibility of discovering such correspondences automatically by analyzing geometries and contact formations.

2.3 Planning

In planning, we are given an environment and an initial state and asked to find a feasible trajectory that satisfies some goal. We solve this problem using the standard framework of constraint-based task and motion planning [6], where a high-level search over sequences of *modes* defines the constraints that will apply at each segment of the trajectory, and a low-level solver attempts to find a feasible trajectory given those constraints. When doing constraint-based task and motion planning with our model, modes are represented as kinematic graphs detailing the geometric relationships that hold between objects in the scene—these graphs are obtained by composing the affordances we learned for each object in the previous section: we describe the high-level search procedure using these graphs in Section 2.3.1. Our approach to the low-level optimization is standard, and we describe it in Section 2.3.2. See Figure 2 for an illustration of the found high-level graph sequence and low-level trajectory in a simple block pushing task.

2.3.1 High-level search

The high-level planning procedure does breadth-first search over kinematic graph sequences to be tested by the continuous solver. The initial kinematic graph $\boldsymbol{G}_0$ is always taken to be such that the movement of actuated objects is unconstrained (there is a free constraint edge between them and the environment), and unactuated objects are taken to be at rest in their initial positions (there is a fixed constraint edge between them and the environment.) The breadth-first search expansion starts from the root node $\boldsymbol{G}_0$ and proceeds by expanding leaf nodes in the tree by either adding or removing a learned affordance using some effector: these two transformations translate to making and breaking contact. Adding an affordance to a graph has two consequences:

- An edge is created between the effector and the target object: that edge's type is given by the affordance's action constraint.
- The edge between the target object and the environment has its type changed to that of the affordance's motion constraint.

For example, in Figure 2, G_0 is transformed by adding an affordance which has a fixed constraint between the gripper and the block and a prismatic constraint between the block and the environment (represented here as the table.) The fixed constraint is added to the graph, whereas the prismatic constraint replaces the constraint that previously existed between the block and the table.

Removing an affordance, on the other hand, removes the constraint between effector and object and restores the object's original constraint to the environment.

Given that the model can either add or remove affordances and that any object other than the target could potentially serve as the effector for an affordance, a simple upper bound on the search tree's branching factor is 2 * number of affordances * (number of objects - 1). In practice the branching factor is a lot lower as affordances can only be removed if they are present in the previous graph.

The search terminates when a sequence of graphs is found that allows for a trajectory satisfying the goal specification. We present an overview of the high-level planner in Algorithm 1:

See figure 2 for an example of a graph sequence found to solve a task. In this case, the initial graph $\boldsymbol{G}_0$ was modified by applying the block's prismatic pushing affordance using the gripper as the effector: this created a fixed constraint between gripper and block and changed the constraint between the block and the table to a prismatic one, resulting in graph $\boldsymbol{G}_1$. The graph sequence ($\boldsymbol{G}_0$, $\boldsymbol{G}_1$) allowed a feasible trajectory that reached the goal (placing the block in the configuration in red in Figure 2, and so the search ended.

Algorithm 1: High-level Planner

Data: G_0, goal, affordances
Result: a graph sequence with a feasible trajectory to the goal
queue $\Leftarrow (G_0)$
while *queue is not empty* **do**
  graphSeq $\Leftarrow$ queue.pop()
  if *feasible* $(graphSeq,\ goal)$ **then**
    return *graphSeq*
  for *affordance* $\in$ *affordances* **do**
    for *effector* $\in$ *objects* $\setminus$ *affordance.target_object* **do**
      $G \Leftarrow$ expand(graphSeq$[-1]$, affordance, effector)
      queue.push(graphSeq $+ (G)$)

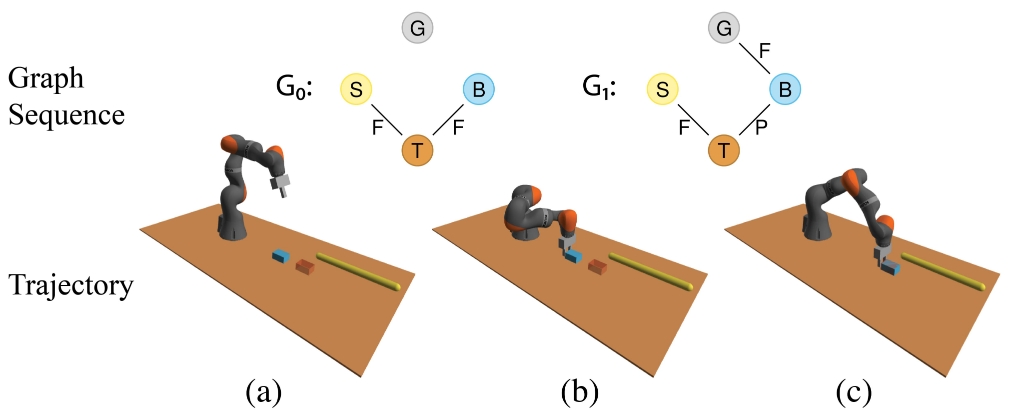

Figure 2: **Task A:** Below: the robot pushes the block along a virtual sliding constraint to the goal configuration. Above: the sequence of graphs constituting the high-level plan for this trajectory: each node represents an object (**G**ripper, **S**tick, **B**lock, and **T**able) and each edge is a virtual or physical constraint between them (**F**ixed or **P**rismatic).

2.3.2 Low-level solver

The high-level search procedure calls the method $feasible$, which verifies that condition 2 holds—that is, that there exists a trajectory that can satisfy the mode constraints given by the sequence of graphs, and that the goal is attainable.

We solve this problem in two steps. First, we check only for task-space feasibility, by ignoring all forward kinematic constraints. This is a computationally cheap procedure, as all the constraints given by the kinematic graph's edges are simple geometric transformations written as matrix multiplications—this allows us to quickly rule out plans that are infeasible or that cannot possibly achieve the goal. If the task-space problem is feasible, we check the full joint-space problem—the procedure is described in detail in the appendix. We use the SQP solver SNOPT [17] for solving the resulting optimization problems.

3 Experiments

Exploration: The model has exploration trials with a block, a stick, and a hook. We describe the grid-search policy for each of these three objects in detail in the appendix. For both the stick and the hook, the robot is made to grasp the tool for the entirety of the trial—this assumption, though limiting, is important as through random exploration one is very unlikely to stumble upon a grasp (unlike a push.) We discuss this limitation and possible extensions in Section 5.

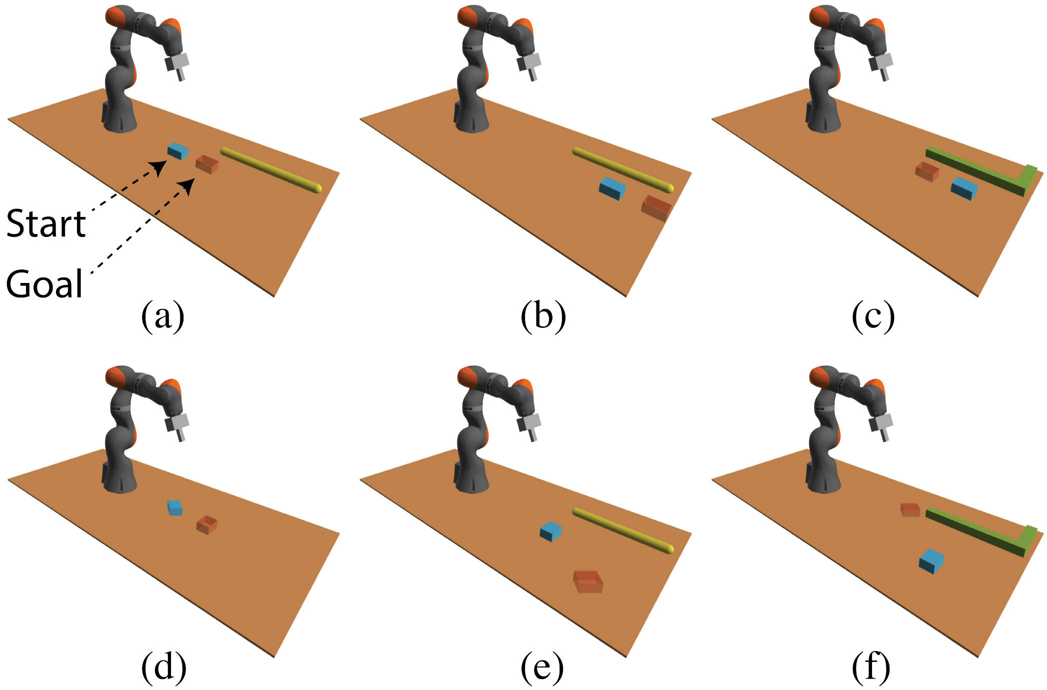

Figure 3: The 6 experimental tasks. Each task requires the robot to move a block from the initial position (cyan) to a goal configuration (red). In scenarios (b), (c), (e), and (f) either the start or goal configurations are outside the kinematic reach of the robot and it needs to use other objects as intermediary tools to create constraints.

The frames on each body used as reference to compute the relative transforms T are a frame at the center of the gripper for the robot, frames located in the handle for the hook and the stick, and the center of mass for the block.

Inference: The MAP affordances learned for each object are described in detail in the appendix. Figure 1 (center) shows the posterior for prismatic and revolute constraints for block motion as a function of contact position (normalized by the max across conditions). Note that the contact enacted in all the interactions in our exploration is sticking: this means that in practice, the relative transform between the gripper and the object remains constant throughout the trial, and the inference procedure infers fixed constraints for them. We found that the priors weighing different types of constraints didn't matter much, so long as they were lower for constraint types with more parameters—this avoids taking sliding motion to be a special case of free motion, for instance. A point that is relevant to the planning procedure that follows has to do with joint states: a prismatic joint in theory allows sliding both forward and backward, but we would like to preclude plans that involve magically ”pulling” an object. Our solution is to define the axes of prismatic and revolute joints to be such that a positive displacement will always have the same direction as the contact normal, and then constrain joint displacements to be positive in our planning procedure.

Planning: We performed experiments on the 6 tasks depicted in Figure 3. We focus on tasks that require using surrounding objects as tools to achieve the desired goal: these tasks naturally involve object-centric and sequential planning. Across the 6 tasks, the robot must reason over sequences of virtual and real constraints and generalize across tools (finger, stick, or hook) to actuated and manipulate the object.

Tasks (a) and (b) require the robot to push a block into the goal configuration by creating a virtual sliding constraint. Task (a) is closest to the exploration phase setup and only requires the robot to reason over how to produce a virtual sliding constraint between the block and table. Figure 2 shows the points at which the robot creates a constraint, representing the transition points between kinematic graphs. In this case, the stick is ignored as reflected in Tab. 1 where the depth of the kinematic graph is 2: the initial configuration and the sliding constraint.

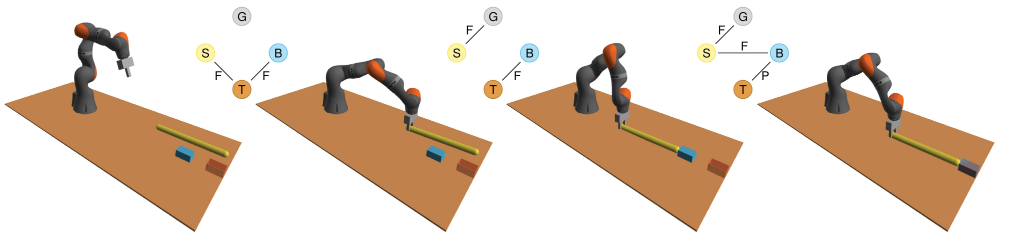

(a) (b) (c) (d)

Figure 4: **Task (b):** Robot uses a stick to push the block along a virtual sliding constraint to the goal configuration – addressing kinematic reach limitations.

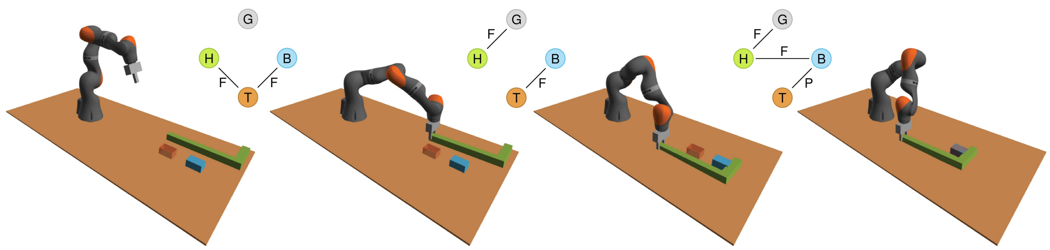

(a) (b) (c) (d)

Figure 5: **Task (c):** Robot pulls the block along a virtual sliding constraint to the goal configuration using a hook – addressing kinematic reach limitations.

The goal configuration in task (b) is outside the kinematic reach of the robot, so it must use the stick as a tool to extend its kinematic reach. Here, the robot needs to generalize the contact formation to the stick tip and push. Figure 4 shows the resulting plan with the additional transition for the robot and stick. We emphasize that the robot has never seen any of the tools being used on the block: it generalizes the contact formations it has seen during exploration to novel interactions it must produce. Tab. 1 shows the additional layer of planning depth required to incorporate the stick.

The start configuration of task (c) lies outside the kinematic reach of the robot. This scenario tests whether the robot can infer that it must pick up the hook in order to create a sliding constraint (from behind) to move the block into position. Figure 5 shows the resulting plan. The planner search depth (table 1) is the same as task (b), where a kinematic check deems the finger push infeasible and the hook is then considered.

Table 1: Solver times and search depth for the tasks.

Task	**solve time (s)**	**solution depth**
A (push)	1.328	2
B (stick push)	1.250	3
C (hook pull)	0.854	3
D (push and rotate)	1.623	4
E (stick push and rotate)	7.106	5
F (hook pull and rotate)	3.066	5

Tasks (d) and (e) are more complex versions of tasks (a) and (b), where the solver needs to incorporate a revolute constraint and both create and destroy virtual constraints in order to get the block to its target configuration, essentially backtracking in order to switch between different kinds of block motion. Figure 6 shows the solution to task (d). We note the transition between panels (c) and (d) where a revolute constraint is switched to a sliding one. The planner incorporates this additional transition with the additional solution depth. The solution to task (e), Figure 7, additionally handles the limitation in kinematic reach by using the stick to actuate the block's sliding constraint.

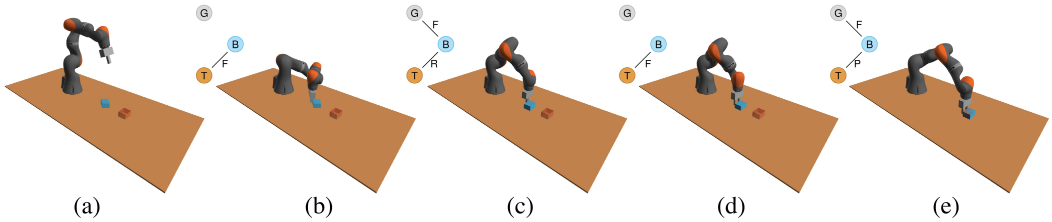

Figure 6: **Task (d):** Robot rotates then pushes the block to the goal configuration.

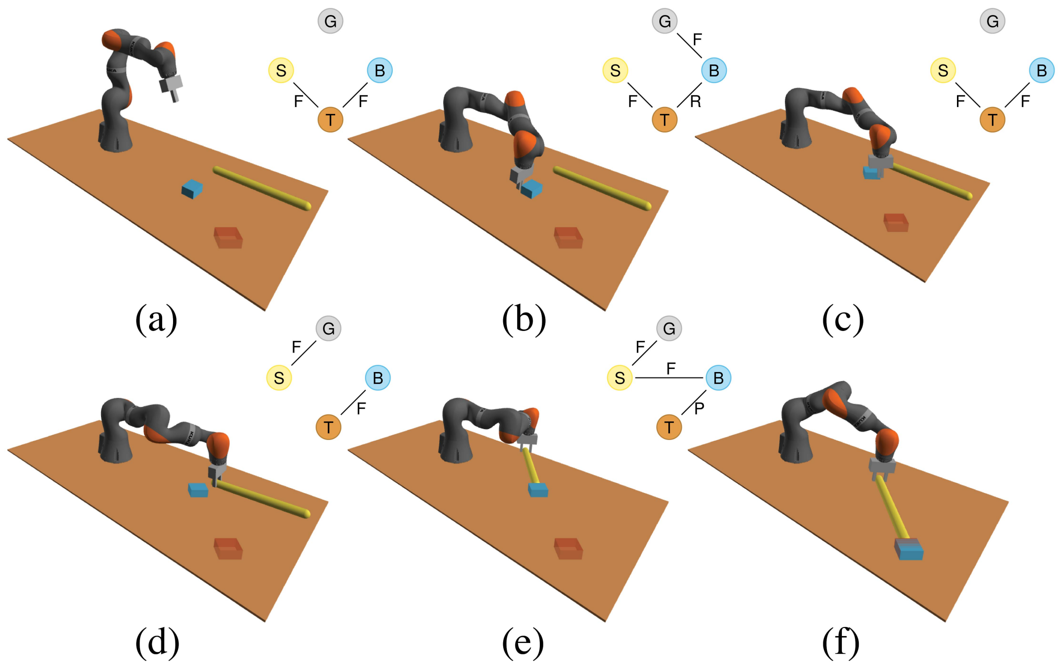

Figure 7: **Task (e):** Robot rotates the block then pushes it to the goal configuration with a stick.

Task (f) is a more challenging iteration of task (c), where the robot has to incorporate an additional rotation with the hook: the model's solution can be seen in Figure Figure 8 The transition between the revolute constraint and the sliding one induced by the stick is occurs between panels (d) and (e) where the robot adjusts the contact formation slightly to facilitate the push action.

The paths shown in Figures 2 through 8 are the first solutions computed by the planner. In principle, the planner could find multiple solutions to a given problem if we allowed it to search beyond the first feasible path. In terms of computational efficiency, a feasible solution was computed in less than 2 seconds for the easier tasks and less than 10 seconds for the hardest (Table 1). The efficiency of the planning method comes from the ability to prune most trajectories at the task level, as they represent infeasible kinematic graph transitions. Therefore, detailed and expensive inverse kinematics only needed to be computed for up to 10 plans in the hardest cases.

Qualitatively, these paths and transition points are highly intuitive. For example, the planner only chooses to use the stick or hook when it cannot reach the block directly. Likewise, when it needs to rotate a block and move it to a position beyond its reach (Figure 7), it does this by first rotating the block with the gripper and then picking the stick up and using it to create a sliding constraint to push the block.

4 Related Work

Besides work on Task and Motion Planning and joint inference that we have mentioned throughout, we identify two other main areas of related work:

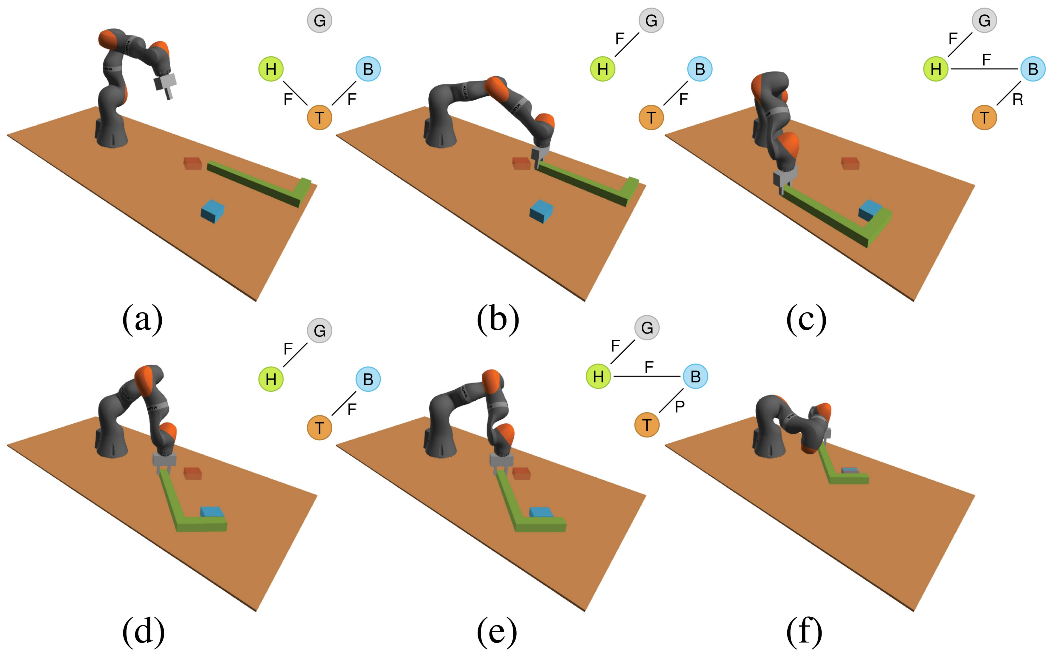

Figure 8: **Task (f):** Robot rotates then pulls the block to the goal configuration with a hook.

Learning for Task And Motion Planning: Learning and inference for TAMP has mostly assumed a set of known, fixed primitives and tried to characterize those to help low-level search (e.g. [16, 18–20]). Conversely, most work in learning primitives has focused on acquiring a single action, and learning a controller for it from experience (e.g. [21–24].) A smaller body of work has attempted to learn primitives as object-oriented skills [25, 26]. [27] learn hybrid models of piecewise-smooth dynamics by modelling transition regions between different modes. [28] use a video dataset of humans doing manipulation tasks to learn a policy that executes natural language instructions describing task plans. [29] use human demonstrations to learn mode transitions, then use RL to learn low-level controllers and a high-level policy.

Planning with simple descriptors for movement: Dynamic Movement Primitives (DMPs) are also a popular method for learning to describe motion [30, 31] where the motion control of the robot is parameterized by attractor dynamics: they are a powerful tool that may be integrated in our framework to facilitate primitive learning. [32] use DMPs to learn finite-state machines from demonstrations by leveraging Bayesian non-parametric models. Similarly to our work, [33] learn to manipulate objects by creating a kinematic models of them, though their approach is restricted to actual joint mechanisms as opposed to virtual joint-like motions.

5 Discussion

Our approach extends kinematic planning to *virtual* constraints, and we showed how this representation can be generalized across novel tool-object interactions, and used to plan in sequential manipulation tasks. We discuss how this fits into the bigger picture of learning for manipulation below:

Learning grasp affordances: Though our work uses a simple exploration policy to learn affordances, these policies are limited when it comes to learning about grasping, as we need to assume exploration trials that start with the robot already holding the relevant object. An interesting extension would be to integrate into the exploration phase an off-the-shelf grasp synthesis algorithm to generate proposals for the exploration policy [34], or an approach for learning to grasp [35].

Reasoning about object geometry: In order to generalize across effectors, we assume knowledge of geometric correspondence across objects, such as between the tip of a finger and the tip of a stick. A promising direction is to automatically discover such keypoints by analyzing geometry: for instance, reasoning that you can cut with an axe's blade and hammer with its blunt edge. Extending our approach with methods to analyze contact formations could narrow this gap [25, 36], and dense object descriptors could help find correspondences between similar objects [37].

Extending Kinematic Constraints: The central emphasis of our approach is on kinematic graphs and constraints. Extending the constraint graph representation to include kinodynamic and dynamic constraints can increase planner expressibility, so we could model e.g. throwing—such representations would also help bring our framework from open-loop planning to closed-loop control. However, this expressibility comes at the cost of more complex control laws and entanglement of abstractions. An interesting middle ground would be allowing for mixed kinematic constraints, such as the simultaneous translation and rotation that occurs in most real-world pushing.

References

[1] L. P. Kaelbling and T. Lozano-Pérez. Hierarchical planning in the now. In *Workshops at the Twenty-Fourth AAAI Conference on Artificial Intelligence*, 2010.

[2] K. Hauser and V. Ng-Thow-Hing. Randomized multi-modal motion planning for a humanoid robot manipulation task. *The International Journal of Robotics Research*, 30(6):678–698, 2011.

[3] F. Lagriffoul, D. Dimitrov, J. Bidot, A. Saffiotti, and L. Karlsson. Efficiently combining task and motion planning using geometric constraints. *The International Journal of Robotics Research*, 33(14):1726–1747, 2014.

[4] S. Srivastava, E. Fang, L. Riano, R. Chitnis, S. Russell, and P. Abbeel. Combined task and motion planning through an extensible planner-independent interface layer. In *2014 IEEE international conference on robotics and automation (ICRA)*, pages 639–646. IEEE, 2014.

[5] N. T. Dantam, Z. K. Kingston, S. Chaudhuri, and L. E. Kavraki. Incremental task and motion planning: A constraint-based approach.

[6] M. Toussaint, K. Allen, K. A. Smith, and J. B. Tenenbaum. Differentiable physics and stable modes for tool-use and manipulation planning. In *Robotics: Science and Systems*, 2018.

[7] C. R. Garrett, T. Lozano-Pérez, and L. P. Kaelbling. Sampling-based methods for factored task and motion planning. *The International Journal of Robotics Research*, 37(13-14):1796–1825, 2018.

[8] F. R. Hogan and A. Rodriguez. Feedback control of the pusher-slider system: A story of hybrid and underactuated contact dynamics. In *Algorithmic Foundations of Robotics XII*, pages 800–815. Springer, 2020.

[9] A. Kloss, M. Bauza, J. Wu, J. B. Tenenbaum, A. Rodriguez, and J. Bohg. Accurate vision-based manipulation through contact reasoning. *arXiv preprint arXiv:1911.03112*, 2019.

[10] M. McCloskey. Naive theories of motion. *Mental models*, pages 299–324, 1983.

[11] M. K. McBEATH and R. N. Shepard. Apparent motion between shapes differing in location and orientation: A window technique for estimating path curvature. *Perception & Psychophysics*, 46(4):333–337, 1989.

[12] E. S. Spelke and K. D. Kinzler. Core knowledge. *Developmental science*, 10(1):89–96, 2007.

[13] J. Sturm, C. Stachniss, and W. Burgard. A probabilistic framework for learning kinematic models of articulated objects. *Journal of Artificial Intelligence Research*, 41:477–526, 2011.

[14] P. R. Barragän, L. P. Kaelbling, and T. Lozano-Pérez. Interactive bayesian identification of kinematic mechanisms. In *2014 IEEE International Conference on Robotics and Automation (ICRA)*, pages 2013–2020. IEEE, 2014.

[15] R. Martín-Martín and O. Brock. Coupled recursive estimation for online interactive perception of articulated objects. *The International Journal of Robotics Research*, page 0278364919848850, 2019.

[16] Z. Wang, C. R. Garrett, L. P. Kaelbling, and T. Lozano-Pérez. Active model learning and diverse action sampling for task and motion planning. In *2018 IEEE/RSJ International Conference on Intelligent Robots and Systems (IROS)*, pages 4107–4114. IEEE, 2018.

[17] P. E. Gill, W. Murray, and M. A. Saunders. Snopt: An sqp algorithm for large-scale constrained optimization. *SIAM review*, 47(1):99–131, 2005.

[18] G. Konidaris, L. P. Kaelbling, and T. Lozano-Perez. From skills to symbols: Learning symbolic representations for abstract high-level planning. *Journal of Artificial Intelligence Research*, 61: 215–289, 2018.

[19] B. Kim, Z. Wang, L. P. Kaelbling, and T. Lozano-Pérez. Learning to guide task and motion planning using score-space representation. *The International Journal of Robotics Research*, 38 (7):793–812, 2019.

[20] R. Chitnis, L. P. Kaelbling, and T. Lozano-Pérez. Learning quickly to plan quickly using modular meta-learning. In *2019 International Conference on Robotics and Automation (ICRA)*, pages 7865–7871. IEEE, 2019.

[21] P. Agrawal, A. V. Nair, P. Abbeel, J. Malik, and S. Levine. Learning to poke by poking: Experiential learning of intuitive physics. In *Advances in neural information processing systems*, pages 5074–5082, 2016.

[22] M. Bauza, F. R. Hogan, and A. Rodriguez. A data-efficient approach to precise and controlled pushing. *arXiv preprint arXiv:1807.09904*, 2018.

[23] J. Mahler, J. Liang, S. Niyaz, M. Laskey, R. Doan, X. Liu, J. A. Ojea, and K. Goldberg. Dex-net 2.0: Deep learning to plan robust grasps with synthetic point clouds and analytic grasp metrics. *arXiv preprint arXiv:1703.09312*, 2017.

[24] J. Mahler, M. Matl, X. Liu, A. Li, D. Gealy, and K. Goldberg. Dex-net 3.0: Computing robust vacuum suction grasp targets in point clouds using a new analytic model and deep learning. In *2018 IEEE International Conference on Robotics and Automation (ICRA)*, pages 1–8. IEEE, 2018.

[25] O. Kroemer and G. S. Sukhatme. Feature selection for learning versatile manipulation skills based on observed and desired trajectories. In *2017 IEEE International Conference on Robotics and Automation (ICRA)*, pages 4713–4720. IEEE, 2017.

[26] O. Kroemer and G. Sukhatme. Meta-level priors for learning manipulation skills with sparse features. In *International Symposium on Experimental Robotics*, pages 211–222. Springer, 2016.

[27] G. Lee, Z. Marinho, A. M. Johnson, G. J. Gordon, S. S. Srinivasa, and M. T. Mason. Unsupervised learning for nonlinear piecewise smooth hybrid systems. *arXiv preprint arXiv:1710.00440*, 2017.

[28] L. Shao, T. Migimatsu, Q. Zhang, K. Yang, and J. Bohg. Concept2robot: Learning manipulation concepts from instructions and human demonstrations.

[29] O. Kroemer, C. Daniel, G. Neumann, H. Van Hoof, and J. Peters. Towards learning hierarchical skills for multi-phase manipulation tasks. In *2015 IEEE International Conference on Robotics and Automation (ICRA)*, pages 1503–1510. IEEE, 2015.

[30] S. Schaal, J. Peters, J. Nakanishi, and A. Ijspeert. Learning movement primitives. In *Robotics research. the eleventh international symposium*, pages 561–572. Springer, 2005.

[31] J. Peters, K. Mülling, J. Kober, D. Nguyen-Tuong, and O. Krömer. Towards motor skill learning for robotics. In *Robotics Research*, pages 469–482. Springer, 2011.

[32] S. Niekum, S. Osentoski, G. Konidaris, S. Chitta, B. Marthi, and A. G. Barto. Learning grounded finite-state representations from unstructured demonstrations. *The International Journal of Robotics Research*, 34(2):131–157, 2015.

[33] D. Katz and O. Brock. Manipulating articulated objects with interactive perception. In *2008 IEEE International Conference on Robotics and Automation*, pages 272–277. IEEE, 2008.

[34] A. Sahbani, S. El-Khoury, and P. Bidaud. An overview of 3d object grasp synthesis algorithms. *Robotics and Autonomous Systems*, 60(3):326–336, 2012.

[35] J. Bohg, A. Morales, T. Asfour, and D. Kragic. Data-driven grasp synthesis—a survey. *IEEE Transactions on Robotics*, 30(2):289–309, 2013.

[36] O. Kroemer and J. Peters. Predicting object interactions from contact distributions. In *2014 IEEE/RSJ International Conference on Intelligent Robots and Systems*, pages 3361–3367. IEEE, 2014.

[37] P. R. Florence, L. Manuelli, and R. Tedrake. Dense object nets: Learning dense visual object descriptors by and for robotic manipulation. *arXiv preprint arXiv:1806.08756*, 2018.

[38] T. Migimatsu and J. Bohg. Object-centric task and motion planning in dynamic environments. *IEEE Robotics and Automation Letters*, 5(2):844–851, 2020.

A Grid-search exploration policies

We describe the grid-search exploration policy used for each object

- **Block:** in the initial position, the block lies on the table. Contact positions are sampled over one of the block's largest lateral surfaces, and the contact force applied is always normal to the contact with unit magnitude.
- **Stick:** in the initial position, the gripper is grasping the stick, which floats above the table. The contact position is fixed as that grasp position, and the force has direction sampled over a 3d grid and unit magnitude.
- **Hook:** same as with the stick.

B Constraint models

We consider four types of kinematic constraint: fixed, sliding, revolute, and free. In this section, we discuss the parametrization and inference of the constraints given observations of interactions (similar to [13]). Consider bodies A and B with body-fixed frames $\mathbf{F}_A$ and $\mathbf{F}_B$. The kinematic constraint between the two bodies relates the transformation between their frames at time t as:

$$\mathbf{F}_A^t = \mathbf{T}^t(\boldsymbol{\theta}, \boldsymbol{\lambda_t})\mathbf{F}_B^t \tag{8}$$

where $\boldsymbol{\theta}$ denotes the constraint parameters, such as the axis of rotation and translation, which is constant in time, and $\boldsymbol{\lambda}_t$ denotes the constraint state, such as the rotation angle or the translation displacement, which can vary in time. Given an exploration phase containing frame trajectories $F_A^{0:T}$ and $F_B^{0:T}$, we want to infer the parameters $\boldsymbol{\theta}$ that, along with a set of states $\boldsymbol{\lambda_{0:T}}$, minimize the sum of the distances between the predicted transformation and the observed transformation, namely:

$$\hat{\boldsymbol{\theta}}, \hat{\boldsymbol{\lambda}}_{0:T} = \underset{\theta, \lambda_{0:T}}{\operatorname{argmin}} \sum_{t=0}^{T} ||\mathbf{F}_A - \mathbf{T}(\boldsymbol{\theta}, \boldsymbol{\lambda_t})\mathbf{F}_B||_F, \tag{9}$$

where $||\cdot||_F$ is the Frobenius norm computed over the transformation matrix. Depending on the constraint type, the optimal parameters can be obtained through a close-form solution or through a non-linear optimization procedure. The parameters for each of the constraint types are:

Fixed: A fixed constraint has parameters $\boldsymbol{\theta} \in R^6$, as a rigid body transform between the two frames containing 3 parameters defining the translation and 3 parameters defining the roll, pitch, and yaw angles. It has no state $\boldsymbol{\lambda_t}$.

Prismatic: A prismatic constraint has parameters $\boldsymbol{\theta} \in R^9$, with a rigid body transform defining the origin of translation, and 3 parameters defining the axis of translation. Additionally, it has a state $\boldsymbol{\lambda_t} \in R$, defining the translational displacement at time t.

Revolute: A revolute constraint has parameters $\boldsymbol{\theta} \in R^6$, with a three parameters defining the rotation center and three parameters defining the axis of rotation. Additionally, it has a state $\boldsymbol{\lambda_t} \in R$, defining the angle of rotation at time t.

Free: A free constraint has no parameters, as it allows for any kind of relative movement between A and B (think for instance of the possible motions of a stick after it's grasped.)

C Learned affordances

The MAP affordances for each object are:

- **Block:**
  - Action: fixed constraint between effector and block's left edge.
    Motion: rotation around an axis normal to the table passing through the block's edge opposite to the contact point.
  - Action: fixed constraint between effector and block's right edge.
    Motion: rotation around an axis normal to the table passing through the block's edge opposite to the contact point.

- Action: fixed constraint between effector and block's center.
  Motion: translation along an axis going from the contact point to the block's center of mass.

- **Stick:**
  - Action: fixed constraint between effector and handle position.
    Motion: free movement relative to the environment.
- **Hook:**
  - Action: fixed constraint between effector and handle position.
    Motion: free movement relative to the environment.

D Continuous Solver Kinematic Check

Let us denote the position of all objects with respect to a fixed world frame at time t by $\boldsymbol{x}_t$, and the position of object i by $\boldsymbol{x}_t^i$. Since a kinematic graph $\boldsymbol{G}$ contains a collection of edges $\boldsymbol{J}$ that represent a constraint between two objects i and j, we can write the set of constraints that G specifies as $J_{ij}(\boldsymbol{x}^i, \boldsymbol{x}^j) = 0, \forall \boldsymbol{J}_{ij} \in E_{G_t}$. Therefore, given a graph sequence $(\boldsymbol{G}_0, \boldsymbol{G}_T)$, where $\boldsymbol{G}_0$ is the initial graph and $\boldsymbol{G}_T$ is the goal graph, we can check for the feasibility of the kinematic transitions and of the goal by solving the following constraint satisfaction problem:

$$\begin{aligned}
\text{find} \quad & \boldsymbol{x}_{0:T},\ \boldsymbol{q}_{0:T} \\
s.t. \quad & \boldsymbol{J}_{ij}(\boldsymbol{x}_t^i, \boldsymbol{x}_t^j) = 0, \\
& \boldsymbol{J}_{ij}(\boldsymbol{x}_{t+1}^i, \boldsymbol{x}_{t+1}^j) = 0, \\
& \boldsymbol{FK}_i(\boldsymbol{q}_i) = \boldsymbol{x}_i, \boldsymbol{FK}_j(\boldsymbol{q}_j) = \boldsymbol{x}_j, \\
& \forall t \in [0, T], \\
& \forall \boldsymbol{J}_{ij} \in \boldsymbol{E}_{G_t},
\end{aligned}$$

where $\boldsymbol{q}_i$ and $\boldsymbol{FK}_i$ are respectively the vector of joint positions and the forward kinematics function for object i.

We solve this problem by first disregarding the forward kinematics constraints, and then solving for joint poses using inverse kinematics. Concurrent work [38] uses a similar two-step approach to get real-time motion replanning, highlighting the efficiency of this formulation. It comes at a price though: since this procedure commits to a task-space plan before checking for kinematic feasibility, it's possible that it will disregard adequate high-level plans because it didn't consider joint information when positing a task-space trajectory. To illustrate this point, consider the task of pulling an object with a hook such that it's close enough for the robot to grasp it. Being close enough to grasp is a condition that only makes sense in joint space: since that information is unavailable to the robot at the time of committing to a task-space plan, the robot will likely settle on a bad task-space plan and consider the problem infeasible once it tries to translate that plan into join-space. A possible workaround is to introduce task-space constraints reflecting the robot's workspace, but in practice none of our experiments involve such corner case conditions, and so we stick with the original formulation.